Intracameral Injection of AAV-DJ.COMP-ANG1 Reduces the IOP of Mice by Reshaping the Trabecular Outflow Pathway

Yunsheng Qiao,[1] Zhongmou Sun,[2] Chen Tan,[1] Junyi Lai,[1] Xinghuai Sun,[1,3,4] and Junyi Chen[1,3,4]

[1]Department of Ophthalmology & Visual Science, Eye & ENT Hospital, Shanghai Medical College, Fudan University, Shanghai, China
[2]University of Rochester, School of Medicine and Dentistry, Rochester, New York, New York, United States
[3]State Key Laboratory of Medical Neurobiology and MOE Frontiers Center for Brain Science, Institutes of Brain Science, Fudan University, Shanghai, China
[4]NHC Key Laboratory of Myopia, Chinese Academy of Medical Sciences, and Shanghai Key Laboratory of Visual Impairment and Restoration (Fudan University), Shanghai, China

Correspondence: Junyi Chen, Department of Ophthalmology, Eye and ENT Hospital of Fudan University, 83 Fenyang Rd., Shanghai 200031, China; chenjy@fudan.edu.cn.

YQ and ZS contributed equally to this work.

Received: June 13, 2022
Accepted: November 24, 2022
Published: December 15, 2022

Citation: Qiao Y, Sun Z, Tan C, Lai J, Sun X, Chen J. Intracameral injection of AAV-DJ.COMP-ANG1 reduces the IOP of mice by reshaping the trabecular outflow pathway. *Invest Ophthalmol Vis Sci.* 2022;63(13):15. https://doi.org/10.1167/iovs.63.13.15

Purpose. The angiopoietin-1 (ANG1)-TIE signaling pathway orchestrates the development and maintenance of the Schlemm's canal (SC). In this study, we investigated the impact of adeno-associated virus (AAV)-mediated gene therapy with cartilage oligomeric matrix protein-ANG1 (COMP–ANG1) on trabecular outflow pathway.

Methods. Different serotypes of AAVs were compared for transduction specificity and efficiency in the anterior segment. The selected AAVs encoding COMP–ANG1 or ZsGreen1 (control) were delivered into the anterior chambers of wild-type C57BL/6J mice. The IOP and ocular surface were monitored regularly. Ocular perfusion was performed to measure the outflow facility and label flow patterns of the trabecular drainage pathway. Structural features of SC as well as limbal, retinal, and skin vessels were visualized by immunostaining. Ultrastructural changes in the SC and trabecular meshwork were observed under transmission electron microscopy.

Results. AAV-DJ could effectively infect the anterior segment. Intracameral injection of AAV-DJ.COMP–ANG1 lowered IOP in wild-type C57BL/6J mice. No signs of inflammation or angiogenesis were noticed. Four weeks after AAV injection, the conventional outflow facility and effective filtration area were increased significantly ($P = 0.005$ and $P = 0.04$, respectively). Consistently, the area of the SC was enlarged ($P < 0.001$) with increased density of giant vacuoles in the inner wall ($P = 0.006$). In addition, the SC endothelia lay on a more discontinuous basement membrane ($P = 0.046$) and a more porous juxtacanalicular tissue ($P = 0.005$) in the COMP–ANG1 group.

Conclusions. Intracamerally injected AAV-DJ.COMP–ANG1 offers a significant IOP-lowering effect by remodeling the trabecular outflow pathway of mouse eyes.

Keywords: AAV, COMP-ANG1, Schlemm's canal, trabecular meshwork

By 2040, 111.8 million people (aged 40–80 years) are estimated to be afflicted with glaucoma, the leading cause of irreversible blindness globally.[1] To date, the only proven and widely practiced treatment to slow or halt the progression of glaucomatous neuropathy is to lower the IOP.[2] IOP is normally kept within narrow acceptable bounds by the balanced aqueous humor (AH) dynamics. It is regulated by the rates of secretion from the ciliary body and drainage through the trabecular and uveoscleral outflow pathways in the iridocorneal angle.[3] Previous studies have demonstrated that IOP elevation in glaucoma patients is associated with increased outflow resistance in the trabecular pathway, mainly comprised of the trabecular meshwork (TM) and the Schlemm's canal (SC).[4,5] And the primary site of resistance generation lies in the immediate vicinity of the inner wall of SC.[6]

The SC is a ring-like, tissue-specific vessel encircling the cornea. Although similarities with both vascular and lymphatic vessels have long been noted,[7] the SC was only recently categorized as a hybrid conduit.[8,9] As in cardiovascular and lymphatic development, the angiopoietin (ANG)–TIE signaling pathway, consisting of two receptors (Tie1 and Tie2, also known as TEK) and three ligands (angiopoietin-1 [ANG1], ANG2, and ANG4), determines the genesis and maintenance of the SC. Conditional deletion of different members in ANG–TIE system leads to SC malformation and glaucomatous phenotypes to varying degrees.[10–13] Also, inhibition of Tie2 activation causes SC regression and IOP elevation in adult mice and monkeys.[11,14] Adding to the clinical significance, TEK and ANG1 loss-of-function mutations have been identified in multiethnic patients with primary congenital glaucoma.[15–17]

Because insufficient ANG–TIE signaling is related to hypoplastic SC and elevated IOP, activation of TIE receptor is a promising therapeutic target for glaucoma. Indeed, some groups have explored the IOP-lowering potential of Tie2 activation by suppression of a negative regulator of Tie2 (vascular endothelial protein tyrosine phosphatase),[18,19] administration of an agonistic antibody[11] and ANG1 recombinant proteins.[12] In this work, sustained expression of a potent ANG1 variant, cartilage oligomeric matrix protein (COMP)–ANG1,[20] was introduced into the anterior segment of adult murine eyes by adeno-associated virus (AAV) vectors. We hypothesized that continuous activation of the ANG-TIE cascade could induce the remodeling of the trabecular pathway (SC in particular) and the reduction of IOP.

Methods

AAV Vectors Construction

AAV-2, AAV-9, AAV-DJ, and AAV–Anc80L65 overexpressing the ZsGreen1 fluorescent protein (Hanbio, Shanghai, China) were initially used to assess the viral transduction efficiency and specificity in the anterior chamber (AC) of naïve eyes (C57BL/6J). The recombinant COMP–ANG1 cDNA containing a secretory signal for hemagglutinin, the coiled-coil domain of rat COMP, the linker and fibrinogen-like domain sequences of human ANG1,[20] and a 3 × Flag (DYKDDDDK) tag was synthesized de novo and incorporated into BamHI/KpnI sites of the pAAV-CMV-MCS-T2A-ZsGreen1 vectors (Hanbio). AAV-DJ with or without COMP–ANG1 were generated by triple transfection system.[21]

Animals and Intraocular Administration

Six-week-old male C57BL/6J (C57) mice were used in this study. All research protocols of animals were approved by the Institutional Animal Care and Use Committee of Eye and ENT Hospital, Fudan University, and in compliance with the ARVO Statement for the Use of Animals in Ophthalmic and Vision Research. C57 mice were randomly assigned to two experimental treatments: the COMP–ANG1 group received AAV-DJ.COMP–ANG1–ZsGreen1 injection in both eyes, and the control group received AAV-DJ.ZsGreen1 injection in both eyes. For intracameral injection, mice were placed under general anesthesia with intraperitoneal injection of ketamine (100 mg/kg) and xylazine (15 mg/kg). We applied 0.2% oxybuprocaine and 0.25% tropicamide (Santen, Osaka, Japan) to dilate the pupils and provide topical anesthesia. Cornea was punctured with a 29-gauge insulin needle (BD Pharmingen, Franklin Lakes, NJ, USA) anterior to the limbus. Two microliters of AAV solution (3×10^9 particles) were delivered into the AC using a microsyringe with a 33G beveled-tip needle (Hamilton, Reno, NV, USA). An additional 1 µL of air was also delivered into the AC to seal the puncture site. For endotoxin-induced uveitis models, 2 µL lipopolysaccharide (100 ng/mL, Sigma-Aldrich, St. Louis, MO, USA) was injected into the AC. Ofloxacin ointment (Sinqi, Shenyang, China) was applied to the surgical eyes before placing the animals on a 37°C heating blanket for recovery.

IOP Measurements

IOP was measured before (24 hours) and after (2, 3, and 4 weeks) intracameral injections using a rebound tonometry (iCare, Espoo, Finland). The mice were acclimatized to awake IOP measurements 2 weeks before AAV injection. To minimize discomfort and facilitate measurements, the cornea was desensitized by applying 2 µL 0.2% oxybuprocaine (Santen) for 1 minute. The researcher then kept the body of a mouse still gently with one hand and the IOP was measured by the other hand. The IOP was calculated as the mean of three steady readings (each reading was the average of six consecutive measurements). All the measurements were taken between 9 AM and 11 AM to avoid bias introduced by diurnal fluctuation of the IOP.

Outflow Facility Measurements

The measurement of outflow facility was based on an established method with minor modifications.[22] Four weeks after AAV delivery, mice from both groups were euthanized by cervical dislocation. Eyes were enucleated within 5 minutes of death and perfused immediately or stored in Dulbecco's modified Eagle's medium (Hyclone, Shanghai, China) at room temperature (26°C) to await perfusion within 2 hours. The experimental setup was developed by our laboratory and was described in details elsewhere.[23] Briefly, the eyes were cannulated by a 33G beveled-tip needle (Nanofil, World Precision Instruments, Shanghai, China) and perfused at increasing pressures (8, 12, 16, and 20 mm Hg) for 10 minutes each. At each pressure, the measurement was repeated at least twice and the perfusion volume was determined as the average. The eyes were kept moisturized by applying PBS drops on top of the cornea every 10 minutes. The room temperature was maintained throughout the experiments. The outflow facility for the trabecular pathway (C_{tra}) was calculated according to Goldmann's equation: $F = C_{tra} \times (IOP - ESP) + F_u$, where F is the rate of AH production, which equals to the perfusion rate in this system. The episcleral venous pressure (ESP) is down to zero ex vivo. And F_u stands for the outflow rate of uveoscleral pathway which is a pressure-independent constant. Under these premises, the C_{tra} could be calculated as the slope of the best fit linear regression to F (perfusion rate) versus IOP (perfusion pressure) data (see the Supplementary Methods for a detailed perfusion protocol and data analysis).

Western Blotting

The iridocorneal angles containing trabecular outflow pathway tissues were carefully dissected in line with a previously reported protocol[24] after 4 weeks of virus inoculation. The tissues were then sonicated and lysed in radioimmunoprecipitation assay buffer (Beyotime, Shanghai, China). Protein concentration were estimated by bicinchoninic acid assay. Eluted protein lysates were loaded and run on 4% to 20% sodium dodecyl sulphate-polyacrylamide gel electrophoresis. Anti–β-actin (1:2000, Proteintech, Wuhan, China) and anti-Flag (DYKDDDDK) (1:2000, Proteintech) were used to assess the overall protein level and COMP–ANG1 expression.

Immunofluorescence Staining

Four weeks after AAV injection, eyes were enucleated and frozen in O.C.T. compound (Tissue-Tek, Sakura, Torrance, CA, USA) immediately. Sagittal sections (12 µm thick) were cut using a cryostat (Leica CM3050 S, Deer Park, IL, USA). For observing virus transduction pattern, green fluorescent signals were imaged using a fluorescence microscopy (DM4000 B, Leica, Wetzlar, Germany) after staining by

Investigative Ophthalmology & Visual Science

4,6-diamidino-2-phenylindole (1 µg/mL; Sigma-Aldrich) for 5 minutes at room temperature. For detection of Flag (DYKDDDDK) tag, sections were fixed with 4% paraformaldehyde for 20 minutes at room temperature. After washing with PBS three times, tissues were permeabilized and blocked (5% goat serum, 0.3% TritonX-100 in PBS) for 1 hour at room temperature and incubated with DYKDDDDK tag rabbit recombinant antibody (1:200, Proteintech) overnight at 4°C. After washing in PBS, sections were incubated with cyanine3-conjugated goat anti-rabbit IgG (Invitrogen, Carlsbad, CA, USA) diluted 1:1000 for 1 hour at room temperature.

Whole-mount immunostaining was performed with fine adjustments to previously published methods.[25,26] Four weeks after AAV injection, eyes were enucleated and immersion fixed in 2% paraformaldehyde overnight at 4°C. After fixation, eyes were separated at the equatorial plane, and the lens as well as remaining retina were removed. The anterior segments were blocked and permeated (5% goat serum, 2.5% bovine serum albumin, 0.5% Triton X-100 in TBS) at room temperature for 6 hours. The samples were then bathed in primary antibody dilutions for at least 48 hours at 4°C. The following primary antibodies were used in this study: anti-CD31 (1:100, Abcam, Cambridge, UK) and anti-LYVE1 (1:100, Abcam). The samples were washed extensively with TBST (0.05% Tween-20 in TBS) six times in 1 hour, followed by incubation with appropriate fluorescent secondary antibodies (Invitrogen) for another 48 hours at 4°C. After six additional washings, samples were trimmed and flat mounted on glass slides with corneal epithelia facing upwards. Images were captured by a Leica SP8 scanning laser confocal microscope (Leica, Wetzlar, Germany). Under fluorescence microscopy, two prominent episcleral venous plexus (EVP) were readily visible in opposite directions, the nearby areas were defined as near EVP regions, and the areas in between were far EVP regions. For SC area measurements, outflow structure reconstruction, and limbal vascular network analysis, we randomly selected one far EVP region of each sample for imaging.

The mouse ears and retina were also harvested at the same time. The posterior skin was peeled away from the intervening cartilage. Subsequent tissue processing and immunostaining procedures were in accord with those of anterior segments. The detailed imaging and analytical process are provided in the Supplementary Methods.

ELISA

The ANG1 level in plasma was quantified using the ANG1 Human ELISA Kit (Abcam) following the manufacturer's instructions. Briefly, 100-µL standards and plasma samples were pipetted into the anti-ANG1 precoated wells and incubated for 2.5 hours at room temperature. The wells were then washed four times and 100 µL biotinylated detection antibody was added for 1 hour incubation at room temperature. After another round of extensive washing, 100 µL horseradish peroxidase-conjugated streptavidin was pipetted to the wells and incubated for 45 minutes at room temperature. The wells were again washed before 100 µL TMB substrate solution was added. The plate was placed in the dark for 30 minutes at room temperature. Finally, 50 µL stop solution was added to cease the reaction and the color intensity was measured at 450 nm immediately using a multimode microplate reader (Tecan, Männedorf, Switzerland).

Transmission Electron Microscopy

Enucleated eyes were immediately immersion-fixed in 2.5% glutaraldehyde for 48 hours at 4°C. The anterior segments were quadrisected before treated with 1% osmium tetroxide and dehydrated by a series of ethanol solutions with increasing concentrations. After resin embedding, ultrathin sagittal sections (70 nm) were produced by Ultramicrotome UC7 (Leica, Wetzlar, Germany) and collected onto copper grids. Images were taken using a JEOL-1230 (80 kV) electron microscope (JEOL, Tokyo, Japan). The SC and TM could be easily identified at the iridocorneal angle. The measurements of SC (including the width, lumen height, and the length of the inner wall) was specified in the Supplementary Methods. The giant vacuoles (GVs) of the inner wall were defined as "smooth-walled, round, oval, reniform, or crescentic spaces," within one cell or forming between two cells of the endothelial lining of SC.[27] Especially, we excluded vacuoles less than 1 μm^2, because it was difficult to distinguish structures that could have been pinocytotic vesicles from small GVs.[6] The area, perimeter, and Feret's diameters of GVs were automatically measured using Fiji.[28] The density of GVs were calculated as the number of GVs per µm of the inner wall. The basement membrane (BM) of the SC endothelia was identified as "a thin line of basal lamina-like structure formed by fine fibrillar and granular material underlying the inner wall endothelium of SC" seen at × 5000 magnification.[29] If only granular material was observed, this region was not included in the measurement of BM length. And the continuity of BM was calculated as: $\frac{BM\ length}{Inner\ wall\ length} \times\ 100\%$. For juxtacanalicular tissues (JCT) porosity measurements, we compared three regions (anterior, intermediate, and posterior) along the JCT with each region 2 µm beneath the inner wall and 14 µm in width, and defined the fraction of open spaces to the JCT area as the porosity (see the Supplementary Methods for details).

Microbeads Infusion and Image Analysis

A 1-mL syringe filled with diluted (1:750) red fluorescent beads (200 nm, amine-modified FluoSpheres, Invitrogen) was secured onto a syringe pump system (Harvard Apparatus, MA, USA). A 32G NovoFine needle (Novo Nordisk, Bagsværd, Denmark) connecting to the syringe was inserted into the ACs of anesthetized mice. Eyes were perfused at a rate of 0.167 µL/min (10 µL/h) for 1 hour. After perfusion, the needle was withdrawn and the mice were maintained for another hour before sacrifice. The anterior segments were harvested and mounted as described above. Aqueous flow pattern was labeled by microbeads trapped in TM and captured by a fluorescent microscope (Leica, Wetzlar, Germany). All samples were imaged together with the same microscope and camera settings. The region of interest selection method and the quantitation of segmental flow were adopted from previous reports[30–32] and were particularized in the Supplementary Methods. Briefly, the original image was first converted to an edge map and was enhanced by applying a circular dilation (size 5). A high area threshold was then set to filter noisy regions in the cornea and iris. Four remaining arc areas representing quadrisected TM/SC regions were selected to calculate effective filtration areas and mean fluorescence intensities (MFI) using Fiji. For segmental flow, the four TM/SC regions were first straightened and then concatenated to show the circumferential distribution of tracers. The MFI along the circumference

Investigative Ophthalmology & Visual Science

were then calculated and the proportions of high flow (distances showing the top one-third of the maximum MFI), low flow (bottom one-third of the maximum MFI), and intermediate flow (middle one-third of the maximum MFI) areas were compared between the groups.

Histological Analysis

Eyes were enucleated and fixed in FAS Eye Fixative (Servicebio, Wuhan, China) for 48 hours at 4°C. Samples were embedded in paraffin, and sagittal sections (5 µm thick) of mice eyes were stained with hematoxylin and eosin for histological evaluation.

Statistical Analysis

Data were analyzed by SPSS statistics 24.0 (IBM Corp., Armonk, NY, USA) and visualized in GraphPad Prism version 6.07 (GraphPad Software, San Diego, CA, USA). Continuous variables conforming to Gaussian distribution were compared using Student *t*-test or Welch's *t*-test (in case of unequal variances). Otherwise, the Mann–Whitney *U* test was applied. IOP deviation from baseline was evaluated using one-way repeated measures ANOVA and the paired Student *t*-test with Bonferroni correction for *P* values. Linear regression analysis was used to calculate the outflow facilities and assess the pressure–resistance relationship in mouse eye perfusion studies. The statistical significance threshold was set to 0.05.

Results

AAV-DJ Can Efficiently Transduce the Anterior Segment Tissues

Initially, we evaluated the infectivity and tissue tropism of four AAV serotypes (AAV-2, AAV-9, AAV-DJ, and AAV-Anc80L65) in the anterior segment (Supplementary Fig. S1). Each viral serotype (3×10^9 particles) carrying ZsGreen1 as a reporter gene was delivered into the ACs of C57 mice. Four weeks later, green fluorescent signals were assessed in cryosectioned ocular slices. Moderate fluorescence was detected in the AC angles of eyes injected with AAV-Anc80L65, while no fluorescent sites can be identified in AAV-2 group. On the contrary, AAV-DJ and AAV-9 showed robust transduction in the cornea (endothelia and stroma, respectively), the iridocorneal angle, and the sclera, indicating active aqueous drainage through both trabecular and uveoscleral pathways. In particular, AAV-DJ showed superior infectivity in the ciliary body where the AH is produced. The transduction pattern of AAV-DJ allows COMP-ANG1 to be not only expressed in outflow structures in situ, but also secreted into the AC by corneal endothelia and ciliary epithelia, and then directed towards the iridocorneal angle. Therefore, we prioritized AAV-DJ to be the optimal vector.

Sustained Expression of COMP-ANG1 Decreased the IOP by Increasing Outflow Facility

After a single injection of viral particles, the IOP of the COMP-ANG1 group was significantly decreased starting

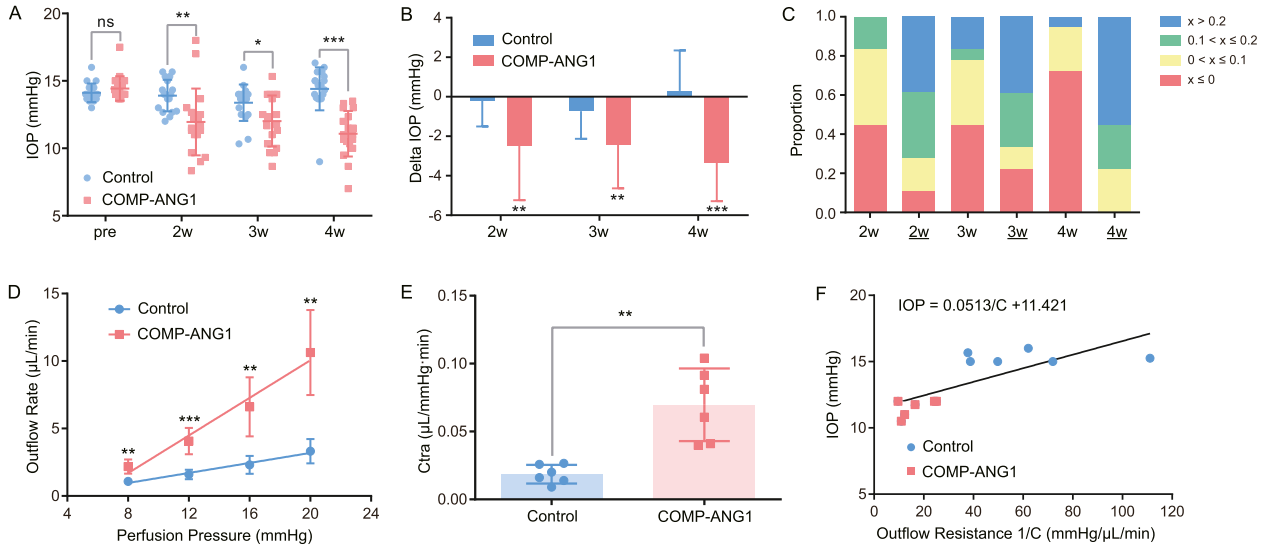

Figure 1. AAV-DJ. COMP-ANG1 inoculation decreased the IOP by increasing trabecular outflow facility. (**A**) IOP levels within four weeks after AAV injection for the COMP-ANG1 group (red squares, $n = 18$ eyes) and the control group (blue dots, $n = 18$ eyes). At each time point after AAV injection, the IOP of the COMP-ANG1 group was lower than that of the control group (pre and 4 weeks: Mann–Whitney *U* test; 2 weeks: Welch's *t*-test; 3 weeks: Student *t*-test). (**B**) Average IOP change from baseline. The IOP was significantly decreased in the COMP-ANG1 group ($n = 18$ eyes) in all postinjection time points (one-way repeated measures ANOVA and paired Student *t*-test with post hoc Bonferroni correction for *P* values), whereas the IOP fluctuation in control mice ($n = 18$ eyes) was not statistically significant. (**C**) Proportion of mice with different levels of IOP reduction in each time point (the *x* axis labels for the COMP-ANG1 group are underlined), *x* = IOP change (%) compared with baseline. (**D**) Relationships between aqueous outflow rate and perfusion pressure in both groups (control, *blue dots*; COMP-ANG1, *red squares*). Straight lines are the best fitting lines. The outflow rates of the COMP-ANG1 group exceeded those of the control group at each perfusion pressure (Welch's *t*-test) (**E**) with increased trabecular outflow facility (C_{tra}). Six eyes from three mice were used for both groups (Welch's *t*-test). (**F**) The IOP measured immediately before death plotted against trabecular outflow resistance ($1/C_{tra}$) measured in the same eyes in the control group (*blue dots*, six eyes from three mice) and the COMP-ANG1 group (*red squares*, six eyes from three mice). The slope of the best fitting line is statistically significant ($P = 0.004$; $R^2 = 0.59$), suggesting that the decreased IOP after AAV-DJ.COMP-ANG1 injection is due in large part to enhanced drainage of the trabecular outflow pathway. Data are presented as mean ± standard deviation (SD) in all panels. ns, not significant. *$P < 0.05$; **$P < 0.01$; ***$P < 0.001$.

from the second week (COMP-ANG1, 11.95 ± 2.47 mm Hg; control, 13.91 ± 1.17 mm Hg; $P = 0.006$; $n = 18$; Welch's *t*-test) and remained reduced compared with the control group throughout the observational period (Fig. 1A). The effect on mean IOP change from baseline is shown in Figures 1B and 1C. Intracameral administration of AAV-DJ.COMP–ANG1 decreased the IOP by 2.4 to 3.4 mm Hg compared with baseline, which was statistically significant at all time points. And more than 65% (66.7%–77.8%) of mice had experienced IOP decrease of more than 10% from baseline. There was no effect of control AAV injection on IOP compared with baseline (mean change from –0.7 to 0.3 mm Hg).

We further tested the effect of COMP-ANG1 expression on outflow facility by ocular perfusion. Eyes were harvested after 4 weeks' inoculation, when IOP was lowered in COMP–ANG1 group (11.08 ± 1.69 mm Hg vs 14.41 ± 1.59 mm Hg in control; $n = 18$; $P < 0.001$; Mann–Whitney *U* test). Flag (DYKDDDDK) signals could be detected in iridocorneal angle tissues by immunofluorescence and Western blotting, confirming the expression of COMP–ANG1 protein (Supplementary Fig. S2). Consistently, the flow rates were increased in AAV-DJ.COMP-ANG1–treated eyes and showed a linear relationship with perfusion pressure (Fig. 1D). The average trabecular outflow facility (C_{tra}) was significantly elevated in the COMP–ANG1 group (0.0697 ± 0.0268 µL/mm Hg·min compared with 0.0186 ± 0.0069 µL/mm Hg·min) measured in control eyes ($n = 6$ in each group; $P = 0.005$; Welch's *t*-test) (Fig. 1E). There was a statistically significant relationship between the IOP measured immediately before sacrifice and the trabecular outflow resistance ($1/C_{tra}$) measured in the same eye ex vivo ($P = 0.004$; $R^2 = 0.59$; $n = 6$ in each group) (Fig. 1F), suggesting that the decreased IOP was attributable to the increased C_{tra}.

COMP–ANG1 Remodels the Trabecular Outflow Structures

Previous investigations have delineated the critical role of ANG–TIE signaling pathway in SC development and maintenance. Therefore, we closely examined the morphological changes of the trabecular outflow pathway. All samples were collected 4 weeks after AAV administration.

The SC area was significantly enlarged in COMP–ANG1 group (0.25 ± 0.01 mm^2 vs 0.18 ± 0.01 mm^2 in controls; four far-EVP regions from four eyes in each group; $P = 0.0001$) (Figs. 2A–2C); both the episcleral vessels and limbal lymphatics networks were structurally indistinguishable between the two groups (Supplementary Fig. S3). We next generated three-dimensional volume renderings of the confocal stacks to visualize outflow structure (Fig. 2D). The XZ plane projections depicted collector channels bridging the superficial episcleral vessels and underlying SCs (Figs. 2E, 2F). The number of collector channels per view (20× objective) and the narrowest diameters of individual CC in XZ plane were measured and compared (Figs. 2G, 2H). Although no significant differences were detected, several expanded anastomoses were observed in the COMP–ANG1 group.

Under transmission electron microscopy, the ultrastructures of SC were clearly identified (Figs. 3A, 3B). As measured in 12 independent sagittal sections (6 sections from 3 eyes in each group), the lumen was wide open in the COMP–ANG1 group, quantified by the cross-sectional area of SC lumen (control, 470.10 ± 346.13 $µm^2$ vs COMP-ANG1, 1327.85 ± 530.42 $µm^2$; $P = 0.016$; Mann–Whitney *U* test) (Fig. 3C) and the lumen height (control, 4.04 ± 3.93 µm vs COMP–ANG1, 11.52 ± 3.39 µm; $P = 0.025$; Mann–Whitney *U* test). Also, the density of GVs in COMP-ANG1 group (0.038 ± 0.012 GV/µm) was higher than that of the control group (0.011 ± 0.014 GV/µm; $P = 0.006$; Student *t*-test) (Fig. 3D). In addition, the average Feret's diameter of GVs in COMP-ANG1 group (2.73 ± 1.41 µm; $n = 47$) was larger than that of GVs in the control group (1.90 ± 0.44 µm; $n = 13$; $P = 0.021$; Mann–Whitney *U* test) (Fig. 3E). The average perimeter of the GVs increased from 6.49 ± 1.60 µm in control mice to 10.09 ± 5.49 µm in AAV-DJ.COMP-ANG1–treated eyes ($P = 0.011$; Mann–Whitney *U* test). Although the mean area of the GVs was also larger in the COMP–ANG1 group (5.79 ± 7.89 $µm^2$ vs 2.45 ± 1.12 $µm^2$ in controls), the change was not statistically significant ($P = 0.09$; Mann–Whitney *U* test). The endothelial monolayer of the SC lies on a discontinuous BM.[33] Interestingly, the activation of ANG–TIE signaling increased the discontinuity of BM manifested by frequent absence of extracellular matrix (ECM) within the layer. The average BM length decreased from 78.5% ± 12.5% of the inner wall length in control mice to 61.2 ± 13.8% in the COMP-ANG1 group ($P = 0.046$; Student *t*-test) (Figs. 3F–3H). In addition, more open spaces were present in the middle JCT in the COMP–ANG1 group (33.4 ± 10.2%) compared with the control group (17.2 ± 4.8%; $P = 0.005$; Student *t*-test) (Figs. 3F, 3G, 3I). Although the average porosity in anterior and posterior JCT were both higher in the COMP–ANG1 group (anterior, 25.7 ± 10.6%; posterior, 17.4 ± 8.5%) compared with control mice (anterior, 17.9 ± 8.0%; posterior, 14.2 ± 4.8%), the differences did not reach the statistical threshold ($P = 0.182$ and 0.200, respectively). To further analyze the functional implications of endothelia and ECM modification, fluorescent tracers were perfused under constant inflow into mouse eyes in vivo. Consistent with an enlarged SC area, the microbeads deposition area (namely, the effective filtration area) was increased in the COMP–ANG1 group (3.68 ± 1.30 mm^2; $n = 8$ eyes) compared with control mice (2.36 ± 1.13 mm^2; $n = 9$ eyes; $P = 0.041$; Student *t*-test) (Figs. 4A, 4B). However, the mean MFI of effective filtration area ($P = 0.712$; Student *t*-test) (Fig. 4C) and the proportions of high flow, intermediate flow, and low flow areas (all $P > 0.05$; Student *t*-test) (Fig. 4D) did not change significantly after AAV injection.

The Safety Profile of Intracameral AAV Delivery

We regularly examined the ocular surface and AC of mice under a slit-lamp microscope. No apparent signs of inflammation or angiogenesis were recorded in either group (Supplementary Fig. S4). No inflammatory infiltration or neovascularization of the cornea, AC angle, vitreous body, and retina was identified by hematoxylin and eosin staining (Fig. 5). We also noted that green fluorescence could be spotted in flat-mounted retina without alterations of the superficial vascular network (Supplementary Fig. S5). Considering COMP–ANG1 was secreted into the AH and ultimately drained into the vascular system, we asked whether the topical injection had systemic effects. ELISA verified that the concentration of ANG1 in circulation was indeed slightly elevated in COMP–ANG1 group (80.2 ± 3.6 pg/mL; $n = 9$) compared with the control group (75.3 ± 2.1 pg/mL;

Investigative Ophthalmology & Visual Science

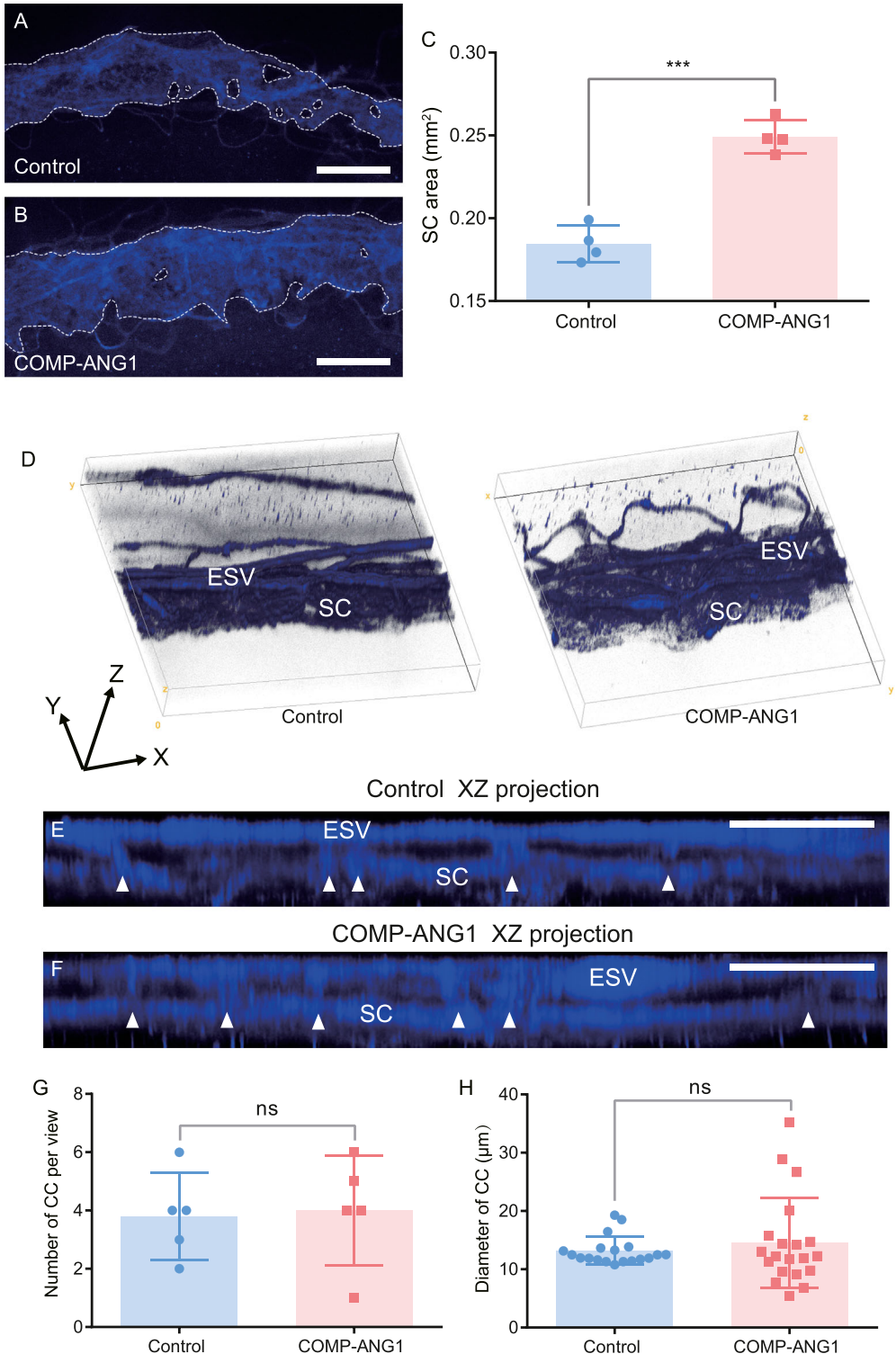

Figure 2. Microscopic structural changes of trabecular outflow pathway after AAV-DJ.COMP-ANG1 injection. CD31 staining was used to delineate the aqueous drainage structures. (**A–C**) The area of SC was significantly increased in the COMP-ANG1 group. The SC area was measured from one randomly selected far-EVP region for each eye (see the Supplementary Methods). Four eyes were analyzed for each group. Dashed lines demarcate SC. Scale bar, 200 μm. (**D**) A 3D rendering of confocal stacks reconstructed the SC and the episcleral vessels (ESV) approximately 20 μm above. (**E and F**) Maximum intensity projection of XZ planes showed two nearly parallel vessel systems, namely, the superficial ESV and the SC underneath, as well as collector channels (CC) bridging the two (indicated by the *arrowhead*). Scale bar, 100 μm. The number of collector channels (CCs) per view (20× objective, one randomly selected far-EVP region for each eye, five views for both groups, Student *t*-test) (**G**) and the narrowest diameter of CCs in XZ plane (measured from images used in G, $n = 19$ for control mice, $n = 20$ for COMP-ANG1 mice, Mann–Whitney *U* test; see the Supplementary Methods for diameter measurements) were comparable between two groups (**H**), although the diameters of CCs in the COMP-ANG1 were more inhomogeneous. Data were presented as mean ± standard deviation in all panels. ns, not significant. ***$P < 0.001$.

Investigative Ophthalmology & Visual Science

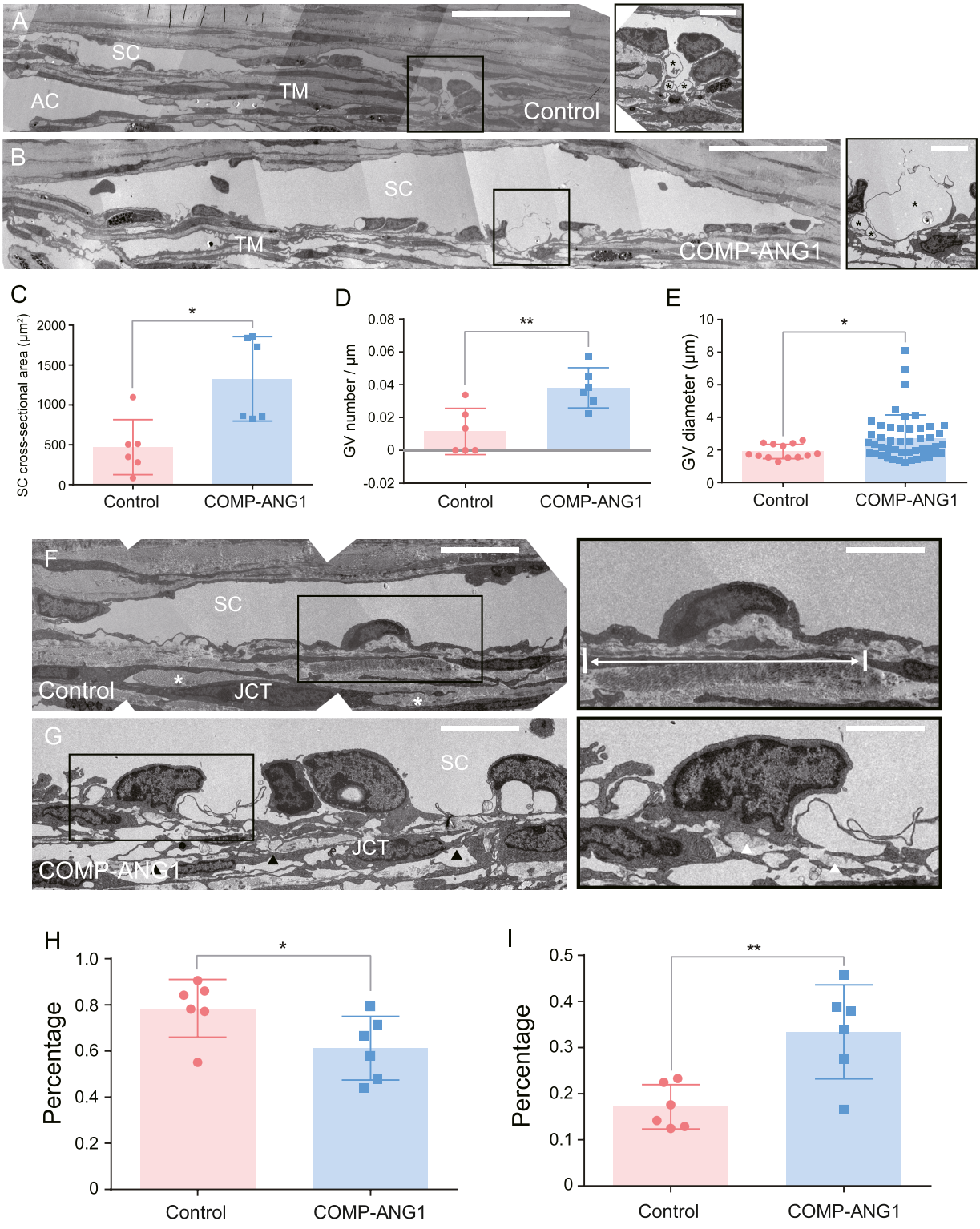

Figure 3. Ultrastructural changes induced by COMP-ANG1 expression in the AC. Two inconsecutive sections from one eye, three eyes from each group were analyzed. (**A and B**) Overviews of the SC and underlying TM. The SC lumen was slit-like in the control group, whereas it was wide open in the COMP-ANG1 group (scale bar in overview images, 25 μm; magnified images, 4 μm). (**C**) Accordingly, the cross-sectional area of SC was significantly larger in the COMP-ANG1 group (Mann–Whitney *U* test). The characteristic outpouching of SC endothelia (GV) was magnified and indicated by *black asterisks*. (**D**) The density of GVs (GV numbers/inner wall length [GV/μm]) was higher in the COMP-ANG1 group (Student *t*-test) with (**E**) larger average Feret's diameters ($n = 13$ GVs for control group, $n = 47$ GVs for COMP-ANG1 group, Mann–Whitney *U* test). (**F and G**) A closer look at the SC endothelia revealed that the BM (identified as a thin basal lamina–like structure immediately underlying the SC inner wall) was more discontinuous in the COMP-ANG1 group, (**H**) as evidenced by the decreased proportion of continuous BM length/total length of SC inner wall (Student *t*-test). (**I**) Interestingly, the porosity of JCT was

higher in the COMP-ANG1 group, as the proportion of open spaces in JCT area increased (Student *t*-test, see the Supplementary Methods for details of quantification). Scale bar in overview images, 12 µm; magnified images, 6 µm. *white asterisks*, extracellular matrices in JCT; *black triangles*, open spaces in JCT; *white triangle*, granular materials. Data were presented as mean ± standard deviation in all panels. $^{*}P < 0.05$; $^{**}P < 0.01$.

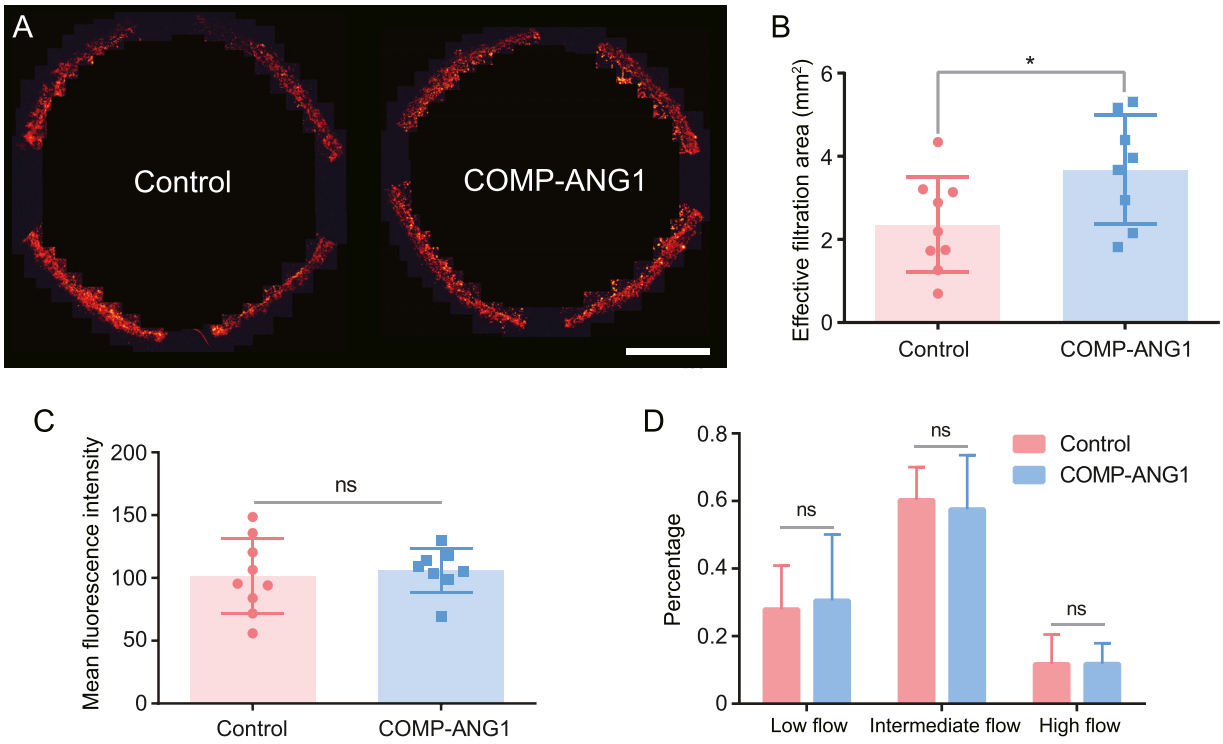

Figure 4. Microbeads deposition in outflow tissues after in vivo perfusion. (**A**) Flat-mounted anterior segments of C57 eyes under fluorescent microscopy after microbeads perfusion (scale bar, 1 mm). The microbeads disposition area (effective filtration area) was measured after the descriptions in Supplementary Methods. Eight and nine whole-mounted anterior segments were measured for the COMP-ANG1 and control groups, respectively. (**B**) There was a significant increase in the effective filtration area of eyes from the COMP-ANG1 group compared with control eyes ($P = 0.041$, Student *t*-test), consistent with an enlarged SC area in the COMP-ANG1 group. (**C**) The mean MFI of effective filtration area showed no statistically significant difference between the two groups. (**D**) Additionally, the aqueous flow pattern (characterized by the proportions of high flow, intermediate flow, and low flow areas, see Supplementary Methods for details) did not change significantly after AAV administration. All results are presented as mean ± standard deviation. ns, not significant. $^{*}P < 0.05$.

n =6; P = 0.011; Student *t*-test). However, no alterations of the vascular or lymphatic networks in ear skins could be detected (Supplementary Fig. S6).

Discussion

A plethora of efficacious antiglaucoma medications have been developed to decrease the IOP, the primary and only modifiable risk factor.[2] First-line treatments function by increasing the uveoscleral AH outflow and/or inhibiting the AH production.[34] However, the resulting AH deprivation from the trabecular outflow pathway is thought to cause the deterioration of the pathway itself and countervail the therapeutic benefit.[35] In recent years, novel medications acting on the conventional pathway, such as Rho kinase inhibitors, were approved for clinical use. However, none of the clinical trials proved them to be superior to existing agents for lowering IOP, necessitating the search for new pharmaceutical targets.[36]

Emerging evidence robustly supports the critical role of the ANG–TIE signaling pathway in the development and maintenance of SC, an essential component of the trabecular outflow system. Genetic deficiency of the ANG–TIE pathway after cardiac formation results in hypoplastic or absent SC and produces ocular hypertension after birth.[10,15] The in vivo discoveries were recapitulated in patients with primary congenital glaucoma with pathogenic TEK and ANG1 mutations.[15,37] Additionally, the activation of TEK cascade is still required to maintain the integrity of SC beyond initial developmental stages. Decreased TEK signaling was observed in aged mice. And depletion of TEK receptor or both its ligands (ANG1 and ANG2) by either conditional knockout or antibody blocking causes SC regression in adult mice and nonhuman primates.[11,14] Interestingly, recent genome-wide association study identified common variants in ANG1 as risk alleles for POAG[38] and TEK mutated patients can sometimes manifest as POAG owing to variable expressivity.[15]

In view of the potential therapeutic application in POAG treatment, several studies have explored the feasibility of decreasing the IOP by activating TEK. Using an ANG2-clustering antibody, ABTAA, which enhances the agonist property of ANG2, Kim et al.[11] showed that the aged SC could be rejuvenated although no alterations of IOP and

Investigative Ophthalmology & Visual Science

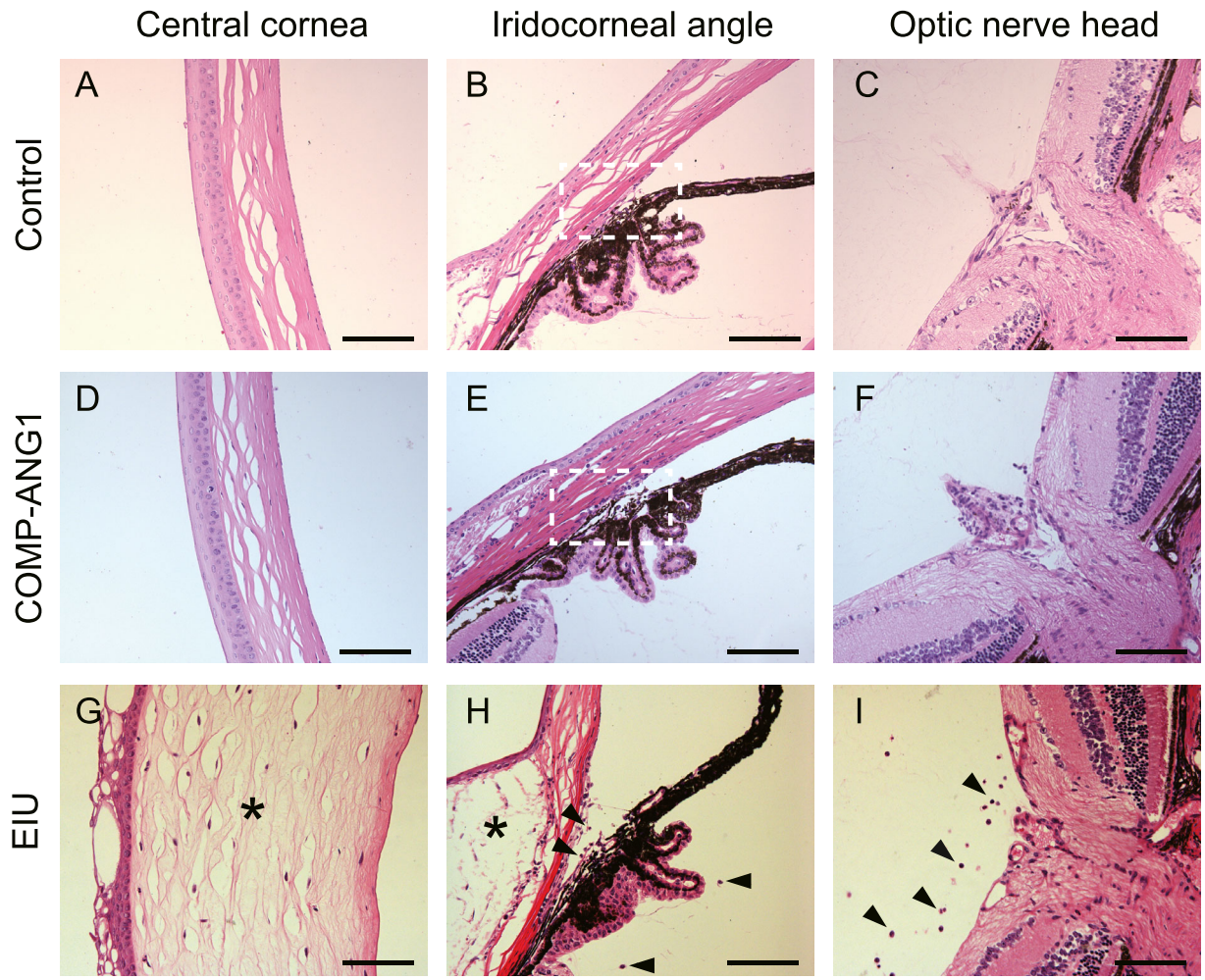

Figure 5. Intracameral injection of AAV-DJ.COMP-ANG1 does not induce evident inflammatory or angiogenic reactions. Hematoxylin and eosin staining showed that the ocular structures of the COMP-ANG1 group ($n = 3$) remained quiescent compared with the control group ($n = 3$) from the cornea to the optic nerve head (**A–F**). In particular, the TM was more porous in the COMP-ANG1 group, consistent with the transmission electron microscopy findings (**B and E**, *white dotted square*). Endotoxin-induced uveitis (EIU) was used as a positive control for inflammation. The cornea and conjunctiva were highly edematous (**G and H**, asterisks). Additionally, neutrophils and mononuclear cells could be found around the ciliary body and the optic nerve head (*arrowheads*). Scale bar, 100 µm. n represents the number of eyes used for paraffin embedding and hematoxylin and eosin staining. Four inconsecutive sections were examined for each eye.

SC area were noted after intravitreal injection. Razuprotafib (AKB-9778), which is a small molecule that activates TEK by inhibiting its negative regulator (vascular endothelial protein tyrosine phosphatase), can decrease the IOP of normotensive diabetic patients, rabbits, and mice through subcutaneous or topical administration.[18] Quaggin et al. recently developed a new ANG1-mimics, Hepta-ANGPT1, which combined the receptor-binding domain of ANG1 and the heptameric scaffold derived from C4-binding protein α. After intravitreal delivery, the IOP was decrease for 3 days in Hepta-ANGPT1–treated wild-type C57 mice. However, no morphological changes of trabecular outflow structures were observed.[12]

In this study, we aimed to investigate the effects of TEK activation sustained by AAV-mediated expression of COMP–ANG1, a designed ANG1 variant. The N-terminal superclustering and coiled-coil oligomeric domains of the original ANG1 are replaced by the short coiled-coil domain of COMP, which makes the recombinant protein more soluble, stable, and potent.[20] Although AAV have been explored extensively as a therapeutical vehicle for inherited retinal diseases,[39,40] its ability to target the anterior segment is less characterized. Therefore, we first compared two naturally occurring AAVs (AAV-2 and AAV-9) and two pseudoserotypes (AAV-DJ and AAV-Anc80L65) for tissue tropism and transduction efficiency in anterior segment tissues. Our results indicated that both AAV-DJ and AAV-9 were significantly superior to the other two serotypes. However, AAV-DJ achieved deeper transduction of the ciliary body compared with AAV-9. AAV-DJ (type 2/8/9 chimera) was created through random homologous recombination and directed evolution.[41] It has a highly efficient gene transfer ability for a broad range of cell types.[42–44] In the eye, AAV-DJ has been shown to be able to efficiently transduce various retinal cells (Müller cells especially) via intravitreal injection as well as primary TM and uveal endothelial cells in vitro.[45,46] Adding to these previous findings, we noted that AAV-DJ could transduce the corneal endothelium and ciliary epithelium, cells demarcating the anterior and posterior chambers, with high efficiency via intracameral injection. Because COMP–ANG1 is a

secretory protein, transduction of the corneal endothelium and ciliary epithelium is supposed to result in the secretion and delivery of the protein to outflow tract by natural aqueous flow. The same strategy has been successfully employed by O'Callaghan et al.[47] in periodic induction of AAV-mediated MMP-3 secretion. Our results further support the feasibility of this strategy which serves as a valuable reference for future research.

Previous studies have shed light on the therapeutic potential of virus delivered COMP-ANG1. Intravitreal injection of AAV2.COMP-ANG1 could attenuate retinal neovascularization and strengthen vascular barrier function in a diabetic mouse model.[48,49] In quiescent vasculature, however, systemic administration of Ad.COMP-ANG1 induces long-lasting vessel enlargement and increased blood flow by promoting endothelial proliferation.[50] Consistent with former reports, we observed significant SC enlargement and amplified aqueous outflow in AAV-DJ.COMP-ANG1–treated eyes reflecting the vascular/lymphatic hybrid nature of SC.[8,9] Thurston et al.[51] previously showed that ANG1 could induce circumferential vessel enlargement restricted to the venous side of the circulation without angiogenic sprouting. They also concluded that this effect only occurs before the fourth postnatal week. From this perspective, SC may be better defined as a vein-like structure with some lymphatic features.[37] Although neither sprouting from the SC nor increase in CC number was noted in this study, the structure of SC and CC was apparently modifiable at the age of 6 weeks, which may be attributed to the enhanced activity of COMP-ANG1 compared with its native form. The morphological changes were quite confined, because the downstream vessels were indistinguishable between the two experimental groups. This could be partly explained by the linker peptide region mediated COMP-ANG1 incorporation into ECM, which reinforced its local action.[52]

It should be noted that the outflow facility of control mice (18 nL/mm Hg·min) measured in this work was higher than that measured using similar setups (6–9 nL/mm Hg·min) in other institutes.[23,53–55] However, previous studies from our lab using the same perfusion equipment and protocol reported consistent measurements in wild-type or control mice (13–18 nL/mm Hg·min).[24,56–59] Comparable facility value (18 nL/mm Hg·min) was also reported by Millar et al.[60] using a constant flow infusion. Because of the small magnitude of the outflow rate in mouse eyes, measurements of the outflow facility are extremely sensitive to subtle systematic differences. The discrepancy in facility measurements is obviously related to the specific instruments used. Therefore, caution should be taken when comparing results reported by different groups. Another factor that could influence the facility value is the temperature. In a temperature-controlled experiments, outflow facility was 2.5-fold greater at eyes bathed in warm saline (17 nL/mm Hg·min; 35°C, mimicking the physiologic temperature) compared with room temperature (7 nL/mm Hg·min; approximately 20°C). The authors extrapolated that a possible temperature-dependent metabolic component could regulate the trabecular outflow in mice.[61] However, studies with temperature-controlled settings (35°C) reported variable facility values (15–29 nL/mm Hg·min).[29,62,63] In this study, the ocular perfusion was conducted at 26°C, which could partly explain the disagreements in facility values. Evaporation from the surface of the perfused eye could also potentially inflated the C_{tra}.[61] We regularly (every 10 minutes) applied PBS to the cornea during perfusion; however, evaporation would still tend to increase the osmolarity at the ocular surface and draw water from the eye.[64] In sum, ocular perfusion generated consistent measurements in our laboratory, and eyes from the control and COMP-ANG1 group were perfused at the same conditions. We, thus, believe that comparisons of C_{tra} between the two groups are meaningful and reasonable.

The outflow facility measured in the COMP–ANG1 group was drastically increased by approximately 274% (compared between the mean C_{tra} of the control and COMP–ANG1 groups), highest among several studies on IOP-lowering treatments.[18,30,47,53,56,65,66] However, we noticed a poor correlation between IOP decreases and facility increases across these studies. Thus, we tried to examine whether the reduction in IOP could be explained by increase in C_{tra} measured in this study. As proposed by Overby et al.,[29] Goldmann's equation predicts a linear relationship between IOP and $1/C_{tra}$ (i.e., trabecular outflow resistance). Accordingly, the IOP measured immediately before death and $1/C_{tra}$ were well-described by a linear relationship (**Fig. 1F**). And the statistical significance of the correlation ($P = 0.004$; $R^2 = 0.59$) suggests that decreased IOP in response to AAV inoculation can be attributed to deceased $1/C_{tra}$ (namely, an increased C_{tra}). Compared with other TEK-activating therapy, the average IOP decrease (–3.35 mm Hg) in the COMP–ANG1 group 4 weeks after AAV injection is similar to those observed at 2 hours after topical application of AKB-9778 (–3.85 mm Hg) and at 24 hours after intravitreal injection of Hepta–ANGPT1 (–3.45 mm Hg),[12,18] suggesting that robust activation of TEK pathway was sustained in AAV-DJ.COMP–ANG1 injected eyes. This was also evidenced by the fact that the SC area increased by approximately 40% at the fourth week after AAV administration compared with 10% after daily treatment of topical AKB-9778 for the same duration.[18] Moreover, the substantial increase in outflow facility is in line with other significant structural alterations, including the enlargement of SC lumen and the increase in GV density and JCT porosity, as well as the disruption of the SC inner wall BM.

The COMP-ANG1–stimulated SC endothelia showed microstructural alterations featured by increased density of GV and sparse BM. The formation of GV is believed to be sensitive to transcellular pressure drop.[67] However, the GVs in vestigial SC of TEK or ANG1/ANG2 deleted mice were almost obliterated despite a significant IOP elevation.[11] Conversely, we observed increased size and density of GVs in mice with a decreased IOP after viral inoculation. These phenomena imply that the ANG–TIE pathway may be engaged in GV regulation in an IOP-independent manner. Notably, ANG1 is known to be an antipermeability agent by strengthening cell junctions.[68] Because the B pores of the SC monolayer are related to cell–cell connectivity,[69] the increase in GV population may indicate AH redirection from decreased or tightened B pores to I pores, which appears in the weakest point of GVs.[70] In addition, the increased discontinuity of SC BM impaired anchoring of endothelial cells to ECM, making the cells more pliable under transcellular pressure.

BM rearrangement is a prerequisite for vessel enlargement.[71] Interestingly, we found that the BM deficiency was limited to the inner wall of SC with coexisting ECM degradation in the adjacent TM. Matrix metalloproteinases (MMPs) are key regulators of ECM turnover in vessel remodeling and trabecular outflow pathway.[72,73] Decreased MMP activity has been related with ECM accumulation and high outflow resistance in glaucomatous eyes.[74] Intracameral injection of

Investigative Ophthalmology & Visual Science

AAV-9.MMP3 results in an increased optically empty space beneath the SC inner wall with enhanced AH outflow facility,[47] reminiscent of the findings in our study. Additionally, ANG1 was shown to induce MMP2, proMMP3, and proMMP9 secretion from porcine pulmonary artery endothelia as well as suppress the expression of tissue inhibitor of metalloproteinase 2.[75] Together, these results suggest that MMPs may participate in the COMP-ANG1–induced ECM regulation, which require further investigation.

There are some limitations to this study. First, because no appropriate POAG animal model is available, we only tested the therapeutic potential of AAV-DJ.COMP–ANG1 in wild-type mice. However, the IOP-lowering effect of COMP-ANG1 in otherwise normal individuals indicates a potent IOP-reducing capacity in hypertensive eyes. Second, we did not report the long-term safety and efficacy profile of the gene-augmentation therapy. Because AAV does not integrate into the host genome, the transduced vectors will be lost gradually.[76] Therefore, prolonged observation should be made to monitor the therapeutic duration of a single injection. Also, it is not clear whether the SC enlargement will persist even after COMP–ANG1 exhaustion. Third, the dose of viral delivery should be further explored and fine-tuned before clinical application.

In summary, we show here that intracameral injection of AAV-DJ.COMP–ANG1 achieves sustained reduction of the AH outflow resistance and IOP in wild-type C57 mice by remodeling the trabecular outflow pathway structures. The current approach gives insights into the therapeutic implication of ANG-TIE activation and serves as a promising candidate for glaucoma treatment.

Acknowledgments

The authors thank Xu Wang and Yu Kong (Institute of Neuroscience, Chinese Academy of Sciences, Shanghai, China) for technical assistance in electron microscopy. We are grateful to Yuan Lei for many useful discussions and invaluable advice.

Supported by grants from the National Natural Science Foundation of China (Grant Numbers: 81870661 & 82171052) and Shanghai Shenkang Hospital Development Center (Grant Number: SHDC12018110). The funding organizations had no role in the design or conduct of this research.

Disclosure: **Y. Qiao**, None; **Z. Sun**, None; **C. Tan**, None; **J. Lai**, None; **X. Sun**, None; **J. Chen**, None

References

1. Tham YC, Li X, Wong TY, et al. Global prevalence of glaucoma and projections of glaucoma burden through 2040: a systematic review and meta-analysis. *Ophthalmology.* 2014;121(11):2081–2090.
2. Jonas JB, Aung T, Bourne RR, et al. Glaucoma. *Lancet.* 2017;390(10108):2183–2193.
3. Carreon T, van der Merwe E, Fellman RL, Johnstone M, Bhattacharya SK. Aqueous outflow - a continuum from trabecular meshwork to episcleral veins. *Prog Retin Eye Res.* 2017;57:108–133.
4. Grant WM. Experimental aqueous perfusion in enucleated human eyes. *Arch Ophthalmol.* 1963;69:783–801.
5. Allingham RR, de Kater AW, Ethier CR. Schlemm's canal and primary open angle glaucoma: correlation between Schlemm's canal dimensions and outflow facility. *Exp Eye Res.* 1996;62(1):101–109.
6. Vahabikashi A, Gelman A, Dong B, et al. Increased stiffness and flow resistance of the inner wall of Schlemm's canal in glaucomatous human eyes. *Proc Natl Acad Sci USA.* 2019;116(52):26555–26563.
7. Ramos RF, Hoying JB, Witte MH, Daniel Stamer W. Schlemm's canal endothelia, lymphatic, or blood vasculature? *J Glaucoma.* 2007;16(4):391–405.
8. Kizhatil K, Ryan M, Marchant JK, Henrich S, John SW. Schlemm's canal is a unique vessel with a combination of blood vascular and lymphatic phenotypes that forms by a novel developmental process. *PLoS Biol.* 2014;12(7):e1001912.
9. Aspelund A, Tammela T, Antila S, et al. The Schlemm's canal is a VEGF-C/VEGFR-3-responsive lymphatic-like vessel. *J Clin Invest.* 2014;124(9):3975–3986.
10. Thomson BR, Heinen S, Jeansson M, et al. A lymphatic defect causes ocular hypertension and glaucoma in mice. *J Clin Invest.* 2014;124(10):4320–4324.
11. Kim J, Park DY, Bae H, et al. Impaired angiopoietin/Tie2 signaling compromises Schlemm's canal integrity and induces glaucoma. *J Clin Invest.* 2017;127(10):3877–3896.
12. Thomson BR, Liu P, Onay T, et al. Cellular crosstalk regulates the aqueous humor outflow pathway and provides new targets for glaucoma therapies. *Nat Commun.* 2021;12(1):6072.
13. Du J, Thomson BR, Onay T, Quaggin SE. Endothelial tyrosine kinase Tie1 is required for normal Schlemm's canal development—brief report. *Arterioscler Thromb Vasc Biol.* 2022;42(3):348–351.
14. Thackaberry EA, Zhou Y, Zuch de Zafra CL, et al. Rapid development of glaucoma via ITV nonselective ANGPT 1/2 antibody: a potential role for ANGPT/TIE2 signaling in primate aqueous humor outflow. *Invest Ophthalmol Vis Sci.* 2019;60(13):4097–4108.
15. Souma T, Tompson SW, Thomson BR, et al. Angiopoietin receptor TEK mutations underlie primary congenital glaucoma with variable expressivity. *J Clin Invest.* 2016;126(7):2575–2587.
16. Kabra M, Zhang W, Rathi S, et al. Angiopoietin receptor TEK interacts with CYP1B1 in primary congenital glaucoma. *Hum Genet.* 2017;136(8):941–949.
17. Qiao Y, Chen Y, Tan C, et al. Screening and functional analysis of TEK mutations in Chinese children with primary congenital glaucoma. *Front Genet.* 2021;12:764509.
18. Li G, Nottebaum AF, Brigell M, et al. A small molecule inhibitor of VE-PTP activates Tie2 in Schlemm's canal increasing outflow facility and reducing intraocular pressure. *Invest Ophthalmol Vis Sci.* 2020;61(14):12.
19. Thomson BR, Carota IA, Souma T, et al. Targeting the vascular-specific phosphatase PTPRB protects against retinal ganglion cell loss in a pre-clinical model of glaucoma. *Elife.* 2019;8:e48474.
20. Cho CH, Kammerer RA, Lee HJ, et al. COMP-Ang1: a designed angiopoietin-1 variant with nonleaky angiogenic activity. *Proc Natl Acad Sci USA.* 2004;101(15):5547–5552.
21. Kimura T, Ferran B, Tsukahara Y, et al. Production of adeno-associated virus vectors for in vitro and in vivo applications. *Sci Rep.* 2019;9(1):13601.
22. Lei Y, Zhang X, Song M, Wu J, Sun X. Aqueous humor outflow physiology in NOS3 knockout mice. *Invest Ophthalmol Vis Sci.* 2015;56(8):4891–4898.
23. Lei Y, Overby DR, Boussommier-Calleja A, Stamer WD, Ethier CR. Outflow physiology of the mouse eye: pressure dependence and washout. *Invest Ophthalmol Vis Sci.* 2011;52(3):1865–1871.
24. Lei Y, Song M, Wu J, Xing C, Sun X. eNOS activity in CAV1 knockout mouse eyes. *Invest Ophthalmol Vis Sci.* 2016;57(6):2805–2813.

25. Thomson BR, Quaggin SE. Morphological analysis of Schlemm's canal in mice. *Methods Mol Biol.* 2018;1846:153–160.
26. Yamazaki T, Li W, Yang L, et al. Whole-mount adult ear skin imaging reveals defective neuro-vascular branching morphogenesis in obese and type 2 diabetic mouse models. *Sci Rep.* 2018;8(1):430.
27. Brilakis HS, Johnson DH. Giant vacuole survival time and implications for aqueous humor outflow. *J Glaucoma.* 2001;10(4):277–283.
28. Schindelin J, Arganda-Carreras I, Frise E, et al. Fiji: an open-source platform for biological-image analysis. *Nat Methods.* 2012;9(7):676–682.
29. Overby DR, Bertrand J, Tektas OY, et al. Ultrastructural changes associated with dexamethasone-induced ocular hypertension in mice. *Invest Ophthalmol Vis Sci.* 2014;55(8):4922–4933.
30. Li G, Mukherjee D, Navarro I, et al. Visualization of conventional outflow tissue responses to netarsudil in living mouse eyes. *Eur J Pharmacol.* 2016;787:20–31.
31. Reina-Torres E, Baptiste TMG, Overby DR. Segmental outflow dynamics in the trabecular meshwork of living mice. *Exp Eye Res.* 2022;225:109285.
32. Vranka JA, Staverosky JA, Raghunathan V, Acott TS. Elevated pressure influences relative distribution of segmental regions of the trabecular meshwork. *Exp Eye Res.* 2020;190:107888.
33. Gong H, Tripathi RC, Tripathi BJ. Morphology of the aqueous outflow pathway. *Microsc Res Tech.* 1996;33(4):336–367.
34. Weinreb RN, Aung T, Medeiros FA. The pathophysiology and treatment of glaucoma: a review. *JAMA.* 2014;311(18):1901–1911.
35. Braunger BM, Fuchshofer R, Tamm ER. The aqueous humor outflow pathways in glaucoma: a unifying concept of disease mechanisms and causative treatment. *Eur J Pharm Biopharm.* 2015;95(Pt B):173–181.
36. Tanna AP, Johnson M. Rho kinase inhibitors as a novel treatment for glaucoma and ocular hypertension. *Ophthalmology.* 2018;125(11):1741–1756.
37. Thomson BR, Souma T, Tompson SW, et al. Angiopoietin-1 is required for Schlemm's canal development in mice and humans. *J Clin Invest.* 2017;127(12):4421–4436.
38. MacGregor S, Ong JS, An J, et al. Genome-wide association study of intraocular pressure uncovers new pathways to glaucoma. *Nat Genet.* 2018;50(8):1067–1071.
39. Maguire AM, Simonelli F, Pierce EA, et al. Safety and efficacy of gene transfer for Leber's congenital amaurosis. *N Engl J Med.* 2008;358(21):2240–2248.
40. Ong T, Pennesi ME, Birch DG, Lam BL, Tsang SH. Adeno-associated viral gene therapy for inherited retinal disease. *Pharm Res.* 2019;36(2):34.
41. Lerch TF, O'Donnell JK, Meyer NL, et al. Structure of AAV-DJ, a retargeted gene therapy vector: cryo-electron microscopy at 4.5 Å resolution. *Structure.* 2012;20(8):1310–1320.
42. Hu X, Wang J, Yao X, et al. Screened AAV variants permit efficient transduction access to supporting cells and hair cells. *Cell Discov.* 2019;5:49.
43. Hickey RD, Lillegard JB, Fisher JE, et al. Efficient production of Fah-null heterozygote pigs by chimeric adeno-associated virus-mediated gene knockout and somatic cell nuclear transfer. *Hepatology.* 2011;54(4):1351–1359.
44. Melo SP, Lisowski L, Bashkirova E, et al. Somatic correction of junctional epidermolysis bullosa by a highly recombinogenic AAV variant. *Mol Ther.* 2014;22(4):725–733.
45. Katada Y, Kobayashi K, Tsubota K, Kurihara T. Evaluation of AAV-DJ vector for retinal gene therapy. *PeerJ.* 2019;7:e6317.
46. Hartzell M, Parker M, Stempel A, et al. Evaluation of AAV-DJ vector as a therapeutic delivery system for ocular cells and tissue. *Invest Ophthalmol Vis Sci.* 2012;53(14):1895–1895.
47. O'Callaghan J, Crosbie DE, Cassidy PS, et al. Therapeutic potential of AAV-mediated MMP-3 secretion from corneal endothelium in treating glaucoma. *Hum Mol Genet.* 2017;26(7):1230–1246.
48. Cahoon JM, Rai RR, Carroll LS, et al. Intravitreal AAV2.COMP-Ang1 prevents neurovascular degeneration in a murine model of diabetic retinopathy. *Diabetes.* 2015;64(12):4247–4259.
49. Carroll LS, Uehara H, Fang D, et al. Intravitreal AAV2.COMP-Ang1 attenuates deep capillary plexus expansion in the aged diabetic mouse retina. *Invest Ophthalmol Vis Sci.* 2019;60(7):2494–2502.
50. Cho CH, Kim KE, Byun J, et al. Long-term and sustained COMP-Ang1 induces long-lasting vascular enlargement and enhanced blood flow. *Circ Res.* 2005;97(1):86–94.
51. Thurston G, Wang Q, Baffert F, et al. Angiopoietin 1 causes vessel enlargement, without angiogenic sprouting, during a critical developmental period. *Development.* 2005;132(14):3317–3326.
52. Xu Y, Yu Q. Angiopoietin-1, unlike angiopoietin-2, is incorporated into the extracellular matrix via its linker peptide region. *J Biol Chem.* 2001;276(37):34990–34998.
53. Stamer WD, Lei Y, Boussommier-Calleja A, Overby DR, Ethier CR. eNOS, a pressure-dependent regulator of intraocular pressure. *Invest Ophthalmol Vis Sci.* 2011;52(13):9438–9444.
54. Boussommier-Calleja A, Bertrand J, Woodward DF, et al. Pharmacologic manipulation of conventional outflow facility in ex vivo mouse eyes. *Invest Ophthalmol Vis Sci.* 2012;53(9):5838–5845.
55. Overby DR, Bertrand J, Schicht M, et al. The structure of the trabecular meshwork, its connections to the ciliary muscle, and the effect of pilocarpine on outflow facility in mice. *Invest Ophthalmol Vis Sci.* 2014;55(6):3727–3736.
56. Tan C, Song M, Stamer WD, et al. miR-21-5p: a viable therapeutic strategy for regulating intraocular pressure. *Exp Eye Res.* 2020;200:108197.
57. Hu C, Zhang Y, Song M, et al. Prolonged use of nitric oxide donor sodium nitroprusside induces ocular hypertension in mice. *Exp Eye Res.* 2021;202:108280.
58. Song M, Wu J, Lei Y, Sun X. Genetic deletion of the NOS3 gene in CAV1-/- mice restores aqueous humor outflow function. *Invest Ophthalmol Vis Sci.* 2017;58(12):4976–4987.
59. Hu C, Niu L, Li L, et al. ABCA1 regulates IOP by modulating Cav1/eNOS/NO signaling pathway. *Invest Ophthalmol Vis Sci.* 2020;61(5):33.
60. Millar JC, Clark AF, Pang IH. Assessment of aqueous humor dynamics in the mouse by a novel method of constant-flow infusion. *Invest Ophthalmol Vis Sci.* 2011;52(2):685–694.
61. Boussommier-Calleja A, Li G, Wilson A, et al. Physical factors affecting outflow facility measurements in mice. *Invest Ophthalmol Vis Sci.* 2015;56(13):8331–8339.
62. Rogers ME, Navarro ID, Perkumas KM, et al. Pigment epithelium-derived factor decreases outflow facility. *Invest Ophthalmol Vis Sci.* 2013;54(10):6655–6661.
63. Boussommier-Calleja A, Overby DR. The influence of genetic background on conventional outflow facility in mice. *Invest Ophthalmol Vis Sci.* 2013;54(13):8251–8258.
64. Johnson M, McLaren JW, Overby DR. Unconventional aqueous humor outflow: a review. *Exp Eye Res.* 2017;158:94–111.
65. Crowston JG, Aihara M, Lindsey JD, Weinreb RN. Effect of latanoprost on outflow facility in the mouse. *Invest Ophthalmol Vis Sci.* 2004;45(7):2240–2245.
66. Li G, Torrejon KY, Unser AM, et al. Trabodenoson, an adenosine mimetic with A1 receptor selectivity lowers intraocular pressure by increasing conventional outflow facility in mice. *Invest Ophthalmol Vis Sci.* 2018;59(1):383–392.
67. Tripathi RC. Mechanism of the aqueous outflow across the trabecular wall of Schlemm's canal. *Exp Eye Res.* 1971;11(1):116–121.

Investigative Ophthalmology & Visual Science

68. Gamble JR, Drew J, Trezise L, et al. Angiopoietin-1 is an antipermeability and anti-inflammatory agent in vitro and targets cell junctions. *Circ Res.* 2000;87(7):603–607.
69. Lai J, Su Y, Swain DL, et al. The role of Schlemm's canal endothelium cellular connectivity in giant vacuole formation: a 3D electron microscopy study. *Invest Ophthalmol Vis Sci.* 2019;60(5):1630–1643.
70. Swain DL, Le TD, Yasmin S, et al. Morphological factors associated with giant vacuoles with I-pores in Schlemm's canal endothelial cells of human eyes: a serial block-face scanning electron microscopy study. *Exp Eye Res.* 2021;205: 108488.
71. Gifre-Renom L, Jones EAV. Vessel enlargement in development and pathophysiology. *Front Physiol.* 2021;12: 639645.
72. Haas TL, Doyle JL, Distasi MR, et al. Involvement of MMPs in the outward remodeling of collateral mesenteric arteries. *Am J Physiol Heart Circ Physiol.* 2007;293(4):H2429–H2437.
73. Acott TS, Kelley MJ, Keller KE, et al. Intraocular pressure homeostasis: maintaining balance in a high-pressure environment. *J Ocul Pharmacol Ther.* 2014;30(2-3):94–101.
74. Nga AD, Yap SL, Samsudin A, et al. Matrix metalloproteinases and tissue inhibitors of metalloproteinases in the aqueous humour of patients with primary angle closure glaucoma - a quantitative study. *BMC Ophthalmol.* 2014;14:33.
75. Kim I, Kim HG, Moon SO, et al. Angiopoietin-1 induces endothelial cell sprouting through the activation of focal adhesion kinase and plasmin secretion. *Circ Res.* 2000;86(9):952–959.
76. Wang D, Tai PWL, Gao G. Adeno-associated virus vector as a platform for gene therapy delivery. *Nat Rev Drug Discov.* 2019;18(5):358–378.

Investigative Ophthalmology & Visual Science